Title
Density characterization of discharged gas-filled capillaries through common-path two-color spectral-domain interferometry.

Journal
Optics Letters, 43(12)

ISSN
0146-9592

Authors
van Tilborg, J
Gonsalves, AJ
Esarey, EH
et al.

Publication Date
2018-06-15

DOI
10.1364/ol.43.002776

Peer reviewed

Optics Letters

Density characterization of discharged gas-filled capillaries through common-path two-color spectral-domain interferometry

J. van Tilborg,* A. J. Gonsalves, E. H. Esarey, C. B. Schroeder, and W. P. Leemans

Lawrence Berkeley National Laboratory, University of California, Berkeley, California 94720, USA
**Corresponding author: JvanTilborg@lbl.gov*

Received 21 March 2018; revised 10 May 2018; accepted 11 May 2018; posted 11 May 2018 (Doc. ID 326244); published 5 June 2018

Electrically discharged plasma structures, typically several centimeters in length and sub-millimeter in diameter, have been applied to guide laser pulses in laser plasma accelerators and to focus ion and relativistic electron beams in compact, radially symmetric transport configurations. Knowledge of the on-axis plasma density is critical. Traditional density interferometry has been ineffective for these laser-machined structures, while group velocity delay (GVD) techniques involve combining two laser paths with corresponding alignment complexities and stability sensitivities. Here the GVD technique is advanced to a common-path two-color interferometer configuration performed in the spectral domain of a broad-bandwidth femtosecond laser. Multi-shot tracking of the phase is not required, and the common path assures improved stability. This *in situ* technique was validated on 15 mm long plasma structures, measuring electron densities of 10^{17}–10^{18} cm^{-3} for various fill pressures.

OCIS codes: (120.3180) Interferometry; (350.5400) Plasmas; (280.5395) Plasma diagnostics; (140.7090) Ultrafast lasers; (190.7110) Ultrafast nonlinear optics.

https://doi.org/10.1364/OL.43.002776

Plasma channels [1–4] play an important role in the intense laser community. Although other approaches towards guiding exist (such as nonlinear self-focusing), pre-formed capillary-based plasma channels [1,5] are well suited to extend the laser-plasma interaction from the diffraction-limited ∼1 mm to several centimeters. Owing to the channel's transverse parabolic density profile, laser pulses can remain guided over many vacuum diffraction lengths. For example, laser plasma accelerators (LPAs) [6] have been demonstrated [7,8] to produce high-quality giga-electron-volt electron beams through the centimeter-scale interaction between an under dense plasma (density ∼10^{18} cm^{-3}) and a relativistic laser pulse (intensity >10^{18} W cm^{-2}). In addition, x-ray lasing [9] and soft x-ray high-harmonic generation [10] have benefited from guiding in pre-formed channels. More recently, discharged plasma structures have been applied to focus relativistic electron beams, exploiting the advantages of radial symmetry, tunability, and strong multi kilo-Tesla/meter focusing gradients [11]. Knowledge of the on-axis plasma density is of critical importance to accelerator applications since the density dominates the plasma response time, self-injection threshold, accelerating field strength, electron beam dephasing length [6], and beam-driven wakefield effects [12].

Traditional time-resolved plasma diagnostics (such as transverse or longitudinal density interferometry) have relied on spatial phase reconstruction of a probe laser pulse, but these techniques have been limited to smooth-walled capillaries of square cross sections, or wide and short capillaries, due to strong optical focusing effects. More recently, Ref. [13] developed the theoretical framework to correlate the group velocity delay (GVD) of a laser pulse to the on-axis plasma density. In experimental demonstrations [14,15], by splitting a femtosecond probe laser into two parts with only one of the pulses traveling through the plasma structure, the density-dependent GVD was recorded through single-shot spectral interferometry of the re-combined pulses. Since ∼1 fs pulse separation diagnostic accuracy is required to retrieve densities of order 10^{17} cm^{-3}, the splitting and re-combination of two laser arms at such precision and stability poses technical challenges.

In this Letter, a novel approach is presented and demonstrated, supplementing the GVD diagnostic with common-path two-color interferometer (TCI; see Refs. [16–23]) concepts. The approach relies on a single femtosecond laser pulse traveling through a frequency-doubling crystal, thus transforming into two co-propagating pulses (the fundamental at frequency ω and the harmonic at 2ω). These two pulses are intrinsically coupled and locked in timing, phase, pointing, and stability, since they experience the same (common) optical path. Following propagation through the plasma, the two pulses build up a phase and envelope shift due to their carrier frequency difference. A second crystal then doubles the fundamental pulse to its 2ω harmonic. Finally, a single-shot spectrum is recorded, delivering the broad-bandwidth modulated spectrum from which both the plasma phase velocity (phase of the spectral fringes) and group velocity (spacing of the spectral fringes) can be retrieved. The common-path TCI efforts to date, including measurements of gas and plasma

densities [20,23], have been performed in the spatial domain (spatial interferometry) and have targeted the phase velocity through fringe tracking. The spectral-domain approach presented in this Letter avoids the necessity for temporal overlap of the pulses (the delay between the two pulses can be quite arbitrary), while the broad-bandwidth-enabled group velocity measurement removes the need for multi-shot phase tracking. Note that this concept is not limited to electrically discharged plasma structures.

The transverse density profile $n(r)$ in a discharged plasma structure [1,5,24] can be defined as

$$n(r) = n_0 + \frac{1}{\pi r_e r_m^4} r^2, \tag{1}$$

with n_0 being the on-axis electron density, r_e being the classical electron radius, and the channel steepness parameter being r_m, also referred to as the matched spot size. The beam size evolution $r_s(z)$ through the capillary [based on a transverse intensity profile $\sim\exp(-2r^2/r_s^2)$] of a laser beam with entrance size r_i has been extensively described in the literature [25]. The on-axis group velocity of the laser pulse in the plasma channel varies during channel propagation z and was derived in appendix B of Ref. [13] to be

$$\frac{v_g(\omega, r_i)}{c} = 1 - \frac{\omega_p^2}{2\omega^2} - \frac{2c^2}{\omega^2 r_m^2}\left[\frac{r_i^2 r_m^2 \sec^2(z/Z_m)}{r_i^4 + r_m^4 \tan^2(z/Z_m)} - \frac{2r_i^2 r_m^2 (r_m^4 - r_i^4)(z/Z_m)\tan(z/Z_m)\sec^2(z/Z_m)}{(r_i^4 + r_m^4 \tan^2(z/Z_m))^2}\right], \tag{2}$$

with c being the vacuum speed of light, λ the laser wavelength, $\omega = 2\pi c/\lambda$, $Z_m = \pi r_m^2/\lambda$, and $\omega_p\ [\mathrm{s}^{-1}] = 5.64 \cdot 10^4 \times \sqrt{n_0\ [\mathrm{cm}^{-3}]}$ the plasma frequency in units of 1/s for on-axis density n_0 in units of cm^{-3}.

By sending a femtosecond probe laser through the first BBO (barium borate, β-BaB_2O_4) crystal (see Fig. 1) two pulses of frequencies ω and 2ω [in our case, $\lambda = 800$ nm ($\omega \rightarrow$"red") and 400 nm ($2\omega \rightarrow$ "blue")] propagate through the capillary. For each pulse, the travel time through a capillary of length L is given by $t(\omega, r_i) = \int_0^L \mathrm{d}z/v_g(\omega, r_i)$. Thus, the temporal walk-off Δt between both pulses can be expressed as $\Delta t = t(\omega, r_{i,\omega}) - t(2\omega, r_{i,2\omega})$. In the regime $k_p r_s \gg 1$ and $r_i \sim r_m$, Eq. (2) is approximately $v_g(\omega)/c \simeq 1 - \omega_p^2/2\omega^2$, and

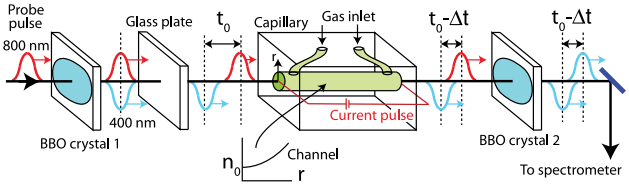

Fig. 1. Schematic concept for the measurement of the on-axis plasma channel density. A fraction of an incoming probe pulse is frequency-doubled in a BBO crystal so that two pulses of different colors (a red pulse at $\lambda = 800$ nm and a blue pulse at $\lambda = 400$ nm) propagate through the plasma channel. The plasma allows the blue pulse to catch up with the red pulse (reduction in delay by Δt). A second BBO crystal converts the red pulse to a second blue pulse, after which an optical spectrometer measures the modulated spectrum of the blue pulses. The change in spectral modulation periodicity is directly related to the on-axis plasma density.

$$\Delta t = \frac{L}{c}\frac{3\omega_p^2}{8\omega^2}. \tag{3}$$

This approximation is valid for typical LPA conditions where $k_p r_s \gg 1$ and near-matched guided is required. For a $\lambda = 800$ nm input probe laser ($\omega = 2.36$ PHz and $2\omega = 4.71$ PHz), Eq. (3) can be expressed numerically as 0.718 fs delay per millimeter of capillary length per 10^{18} cm^{-3} of on-axis density. For example, one can retrieve a $\Delta t = 21.5$ fs slippage for an $L = 15$ mm capillary at $n_0 = 2 \cdot 10^{18}$ cm^{-3}. For illustration purposes, the temporal walk-off between red and blue pulses is studied for the parameters $L = 15$ mm, $r_m = 50\,\mu$m, $r_{i,\omega} = 70\,\mu$m, and $r_{i,2\omega} = 45\,\mu$m. The spot size evolution of both pulses is plotted in the inset Fig. 2(a). For these laser and capillary parameters, Fig. 2(b) displays the overestimation of the retrieved versus actual on-axis density when using the approximated expression Eq. (3), instead of the full treatment based on Eq. (2). For densities above $>5 \cdot 10^{17}$ cm^{-3}, the overestimation error is below 20%. At larger r_m, this error is further reduced.

For an experimental demonstration, the setup depicted in Fig. 1 was developed. A weak laser pulse (several micro-Joules, 45 fs duration, at intensity below ionization threshold for H_2) was incident on a type-I frequency-doubling BBO crystal (thickness 0.1 mm, diameter 10 mm). The fundamental red pulse and the frequency-doubled blue pulse (similar pulse duration) travelled through a piece of 1 mm thick glass to provide a constant temporal offset $t_0 = 250$ fs between both pulses (blue trailing the red pulse). Then both pulses entered an H_2-filled capillary of $L = 15$ mm length and 0.25 mm in diameter. The neutral pressure calibration inside the capillary was measured by sealing off one gas inlet feed and attaching a capacitance manometer to the nearest capillary end. Due to the symmetry of the capillary and gas feed tubes, the calibration can be used to obtain the pressure in the capillary when the gas feed and capillary exit tubes are not sealed. The discharge current

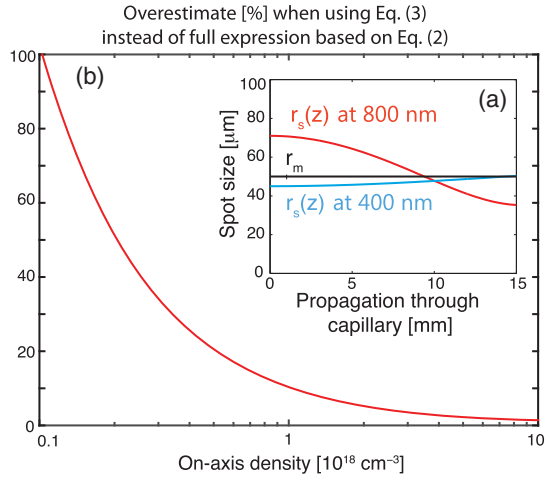

Fig. 2. (a) Evolution of the spot size of the red (ω) and blue (2ω) pulses through a channel with the matched spot size $r_m = 50$ μm. Both pulses experience spot size oscillations. (b) Overestimation of the retrieved versus actual on-axis density when using the approximated expression Eq. (3), instead of the full treatment based on Eq. (2). For densities above $>5 \cdot 10^{17}$ cm^{-3}, the relative error is below 20%.

pulse (see Fig. 4(a) at peak current of 350 A), was measured for each shot. For the probe laser, beam sizes of $r_{i,\omega} = 71$ μm (red pulse) and $r_{i,2\omega} = 47$ μm (blue pulse) were measured. The vacuum focal locations of both pulses were nearly identical due to the long (2 m) focal length of the final focusing optic used upstream of the capillary, although Ref. [13] presented the framework for generalizing v_g for arbitrary capillary entrance divergence. The capillary had a matched spot size of $r_m = 48$ μm as studied in Ref. [26].

As was presented earlier, the change in group velocity induced by the plasma allows the 2ω pulse to catch up with the ω pulse, yielding a modified delay $(t_0 - \Delta t)$. After the capillary, a second type-I BBO crystal (thickness 0.1 mm, diameter 10 mm) was inserted to convert the leading red pulse into a leading blue pulse. The temporal separation was then recorded through measurement of interference oscillations in the optical spectrum of the 2ω pulses. Note that the two BBO crystals and the glass plate in Fig. 1 were positioned within a few centimeters from the capillary on translation stages for easy insertion/removal. With two blue pulses propagating into the optical spectrometer at temporal separation $(t_0 - \Delta t)$, a spectral modulation at periodicity $\delta f = 1/(t_0 - \Delta t)$ is induced. Without a glass plate (so that $t_0 \to 0$), and approximating Δt on the order of 10 fs, the spectral modulation periodicity would be greater than the bandwidth of the 2ω pulses, making it impossible to measure the periodicity δf. However, by having the glass plate in the optical path (so that $t_0 \approx 250$ fs), we find $\delta f \approx 4$ THz which is well within the ≈40 THz bandwidth of the blue pulse.

The spectrometer used for this Letter was an f/4.0 Bruker Optics imaging spectrometer, model 250IS/m. The 150 gr/mm grating was selected, as was an input slit opening of 10 μm. The two co-propagating 2ω pulses were imaged onto the spectrometer entrance slit through a vacuum chamber window. The camera used to record the spectra had a 0.092 nm/pixel spectral calibration, while a line-source-calibrated spectral resolution of 0.8 nm (full width at half-maximum) was measured. A typical single-shot spectral measurement is shown in Fig. 3(a). The line-out shown is an integration of the counts over 40 pixels in the nondispersive plane of the spectral image (see inset). The discrete Fourier transformation (FT) of the line-out is plotted in Fig. 3(b). By temporarily removing the capillary (all other components remained in place) and repeating the measurement, we were able to obtain the fixed t_0 offset.

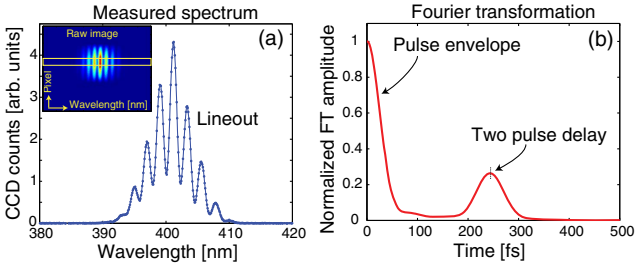

Fig. 3. (a) Typical single-shot line-out of the spectrum of two blue pulses. (The inset shows a raw 2D image.) (b) FT of the raw spectrum shows a side peak around 240 fs, which represents the temporal separation of both pulses. This temporal separation is a function of plasma density in the capillary, hence its usefulness as a density diagnostic.

In order to study the measured on-axis plasma density as a function of neutral gas pressure, a scan was performed where the inlet pressure was varied. The probe laser timing was 192 ns; see the trace shown in Fig. 4(a). Within each 5 Torr bin, all N data points were averaged to $\overline{n_0}$ and error bar σ following $\sigma^2 = (1/N)\sum_{i=1}^{N}(\overline{n_0} - n_{0,i})^2$. When averaging $N = 5$ shots, σ was found to be less than 1 fs. Figure 4(b) displays a monotonic decreasing temporal separation versus pressure, indicating that the leading red pulse is slipping back towards the trailing blue pulse at higher plasma densities. Although the approximated Eq. (3) could have been applied with little error, we used the full expression of Eq. (2) to convert the temporal separation to capillary-length-averaged on-axis density. The capillary-out reference measurement determined that $t_0 = 243.5$ fs. Figure 4(c) shows the retrieved on-axis density. For example, at 46 Torr of neutral H_2, the atomic hydrogen density is $2.9 \cdot 10^{18}$ cm^{-3}. Based on scaling laws discussed by Gonsalves *et al.* [5] for full ionization, an on-axis density of $1.4 \cdot 10^{18}$ cm^{-3} was predicted. Figure 4(c) retrieved a value of $\sim 1 \cdot 10^{18}$ cm^{-3} at 46 Torr. Although in approximate quantitative agreement, possible explanations for the discrepancy are that the scaling laws in Ref. [5] were derived for square (and not circular) capillaries, and/or that the discharge current pulse in Ref. [5] was a different shape, duration, and amplitude. Note that Fig. 4 in Ref. [15], obtained with GVD based on interferometry of two 800 nm pulses, also retrieved $\sim 1 \cdot 10^{18}$ cm^{-3} at 45 Torr for a similar discharge pulse (the capillary was twice the diameter, which has a negligible effect on density.) These results indicate that our diagnostic delivers an accurate value for the on-axis density, providing a useful benchmark for various models and simulations [24,27].

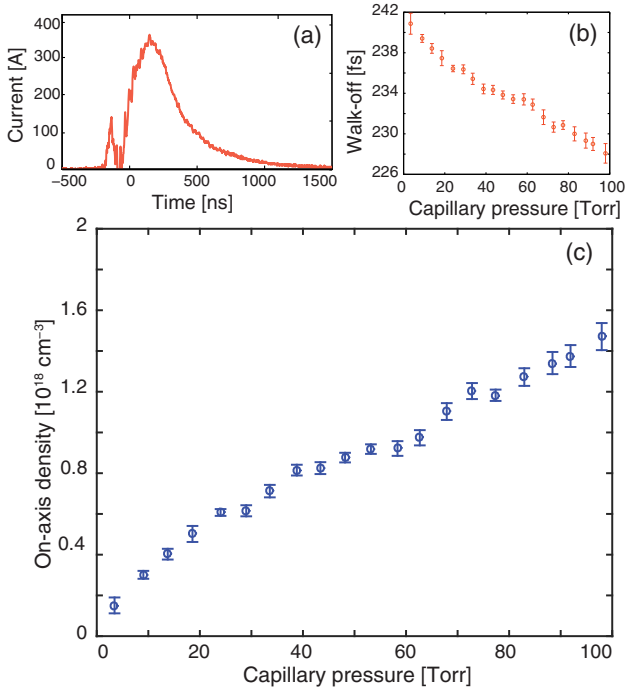

Fig. 4. (a) Temporal profile of the discharge pulse. (b) Measured temporal separation $(t_0 - \Delta t)$ between both 2ω pulses as a function of neutral H_2 pressure in the capillary. By removing the capillary from the setup, the offset delay t_0 was measured to be 243.5 fs. The main figure (c) shows the derived on-axis density n_0, obtained using Eq. (2).

Note that the beam sizes of the ω and 2ω beams on the second BBO crystal (see Fig. 1) will independently vary as a function of the capillary guiding parameters [25]. Being a nonlinear effect, frequency doubling can lead to variations of the relative energy of both pulses entering the spectrometer, thus affecting the fringe contrast. Although the GVD-based density retrieval works even at low fringe contrast, optimally tuning the relative energies of both pulses through BBO crystal rotation will benefit the diagnostic range.

In conclusion, we have developed and demonstrated an *in situ* technique to measure the on-axis density in electrically discharged capillary channels. This knowledge is critical to LPA optimization and particle beam transport applications. The technique relies on the change in temporal separation Δt of co-propagating 800 and 400 nm pulses, derived from a single input laser beam, which can be measured with an optical spectrometer at sub-femtosecond accuracy. Although the exact expression relating Δt to the on-axis density was presented by Eq. (2), we have shown that the approximation of $\Delta t = 0.718$ fs per millimeter of capillary per 10^{18} cm^{-3} of density is an excellent estimate for densities above $>5 \cdot 10^{17}$ cm^{-3}. Density measurements on a 15 mm long H_2-filled capillary at various pressures were presented.

Funding. U.S. Department of Energy (DOE) (DE-AC02-05CH11231); National Science Foundation (NSF) (PHY-1632796); Gordon and Betty Moore Foundation (GBMF4898).

REFERENCES

1. D. J. Spence and S. M. Hooker, Phys. Rev. E **63**, 015401 (2000).
2. A. Butler, D. J. Spence, and S. M. Hooker, Phys. Rev. Lett. **89**, 185003 (2002).
3. C. McGuffey, M. Levin, T. Matsuoka, V. Chvykov, G. Kalintchenko, P. Rousseau, V. Yanovsky, A. Zigler, A. Maksimchuk, and K. Krushelnick, Phys. Plasmas **16**, 113105 (2009).
4. H. M. Milchberg, T. R. Clark, C. G. Durfee III, T. M. Antonsen, Jr., and P. Mora, Phys. Plasmas **3**, 2149 (1996).
5. A. J. Gonsalves, T. P. Rowlands-Rees, B. H. P. Broks, J. J. A. M. van der Mullen, and S. M. Hooker, Phys. Rev. Lett. **98**, 025002 (2007).
6. E. Esarey, C. B. Schroeder, and W. P. Leemans, Rev. Mod. Phys. **81**, 1229 (2009).
7. W. P. Leemans, B. Nagler, A. J. Gonsalves, C. Tóth, K. Nakamura, C. G. R. Geddes, E. Esarey, C. B. Schroeder, and S. M. Hooker, Nat. Phys. **2**, 696 (2006).
8. S. Karsch, J. Osterhoff, A. Popp, T. P. Rowlands-Rees, Z. Major, M. Fuchs, B. Marx, R. Hörlein, K. Schmid, L. Veisz, S. Becker, U. Schramm, B. Hidding, G. Pretzler, D. Habs, F. Grüner, F. Krausz, and S. M. Hooker, New J. Phys. **9**, 415 (2007).
9. A. Butler, A. J. Gonsalves, C. McKenna, D. J. Spence, S. Hooker, S. Sebban, T. Mocek, I. Bettaibi, and B. Cros, Phys. Rev. Lett. **91**, 205001 (2003).
10. D. M. Gaudiosi, B. Reagan, T. Popmintchev, M. Grisham, M. Berrill, O. Cohen, B. C. Walker, M. M. Murnane, H. C. Kapteyn, and J. J. Rocca, Phys. Rev. Lett. **96**, 203001 (2006).
11. J. van Tilborg, S. Steinke, C. G. R. Geddes, N. H. Matlis, B. S. Shaw, A. J. Gonsalves, J. V. Huijts, K. Nakamura, J. Daniels, C. B. Schroeder, S. S. Bulanov, N. A. Bobrova, P. V. Sasorov, and W. P. Leemans, Phys. Rev. Lett. **115**, 184802 (2015).
12. J. van Tilborg, S. K. Barber, C. Benedetti, C. B. Schroeder, F. Isono, H.-E. Tsai, C. G. R. Geddes, and W. P. Leemans, Phys. Plasmas **25**, 056702 (2018).
13. C. B. Schroeder, C. Benedetti, E. Esarey, J. van Tilborg, and W. P. Leemans, Phys. Plasmas **18**, 083103 (2011).
14. J. van Tilborg, J. Daniels, A. J. Gonsalves, C. B. Schroeder, E. Esarey, and W. P. Leemans, Phys. Rev. E **89**, 063103 (2014).
15. J. Daniels, J. van Tilborg, A. J. Gonsalves, C. B. Schroeder, C. Benedetti, E. Esarey, and W. P. Leemans, Phys. Plasmas **22**, 073112 (2015).
16. F. A. Hopf, A. Tomita, and G. Al-Jumaily, Opt. Lett. **5**, 386 (1980).
17. S. P. Velsko and D. Eimerl, Appl. Opt. **25**, 1344 (1986).
18. E. Abraham, K. Minoshima, and H. Matsumoto, Opt. Commun. **176**, 441 (2000).
19. P. Burdack, M. Tröbs, M. Hunnekuhl, C. Fallnich, and I. Freitag, Opt. Express **12**, 644 (2004).
20. P. A. Bagryansky, A. D. Khilchenko, A. N. Kvashnin, A. A. Lizunov, R. V. Voskoboynikov, A. L. Solomakhin, H. R. Koslowski, and T. Team, Rev. Sci. Instrum. **77**, 053501 (2006).
21. H. Yasuaki, Y. Takeshi, and T. Araki, Opt. Rev. **13**, 29 (2006).
22. F. Brandi and F. Giammanco, Opt. Express **19**, 25479 (2011).
23. F. Brandi, F. Giammanco, F. Conti, F. Sylla, G. Lambert, and L. A. Gizzi, Rev. Sci. Instrum. **87**, 086103 (2016).
24. N. A. Bobrova, A. A. Esaulov, J. Sakai, P. V. Sasorov, D. J. Spence, A. Butler, S. M. Hooker, and S. V. Bulanov, Phys. Rev. E **65**, 016407 (2001).
25. E. Esarey and W. P. Leemans, Phys. Rev. E **59**, 1082 (1999).
26. A. J. Gonsalves, K. Nakamura, C. Lin, J. Osterhoff, S. Shiraishi, C. B. Schroeder, C. G. R. Geddes, C. Tóth, E. Esarey, and W. P. Leemans, Phys. Plasmas **17**, 056706 (2010).
27. B. H. P. Broks, K. Garloff, and J. J. A. M. van der Mullen, Phys. Rev. E **71**, 016401 (2005).